A Geometric Construction of Traveling Waves in a Bioremediation Model

M. Beck,[1] A. Doelman,[2] and T. J. Kaper[1]

[1] Department of Mathematics and Statistics, Boston University, Boston, MA 02215, U.S.A.

[2] Centrum voor Wiskunde en Informatica, 1090 BG Amsterdam, the Netherlands

Summary. Bioremediation is a promising technique for cleaning contaminated soil. We study an idealized bioremediation model involving a substrate (contaminant to be removed), electron acceptor (added nutrient), and microorganisms in a one-dimensional soil column. Using geometric singular perturbation theory, we construct traveling waves (TW) corresponding to the motion of a biologically active zone, in which the microorganisms consume both substrate and acceptor. For certain values of the parameters, the traveling waves exist on a three-dimensional slow manifold within the five-dimensional phase space. We prove persistence of the slow manifold under perturbation by controlling the nonlinearity via a change of coordinates, and we construct the wave in the transverse intersection of appropriate stable and unstable manifolds in this slow manifold. We study how the TW depends on the half-saturation constants and other parameters and investigate numerically a bifurcation in which the TW loses stability to a periodic wave.

1. Introduction

In situ bioremediation is a promising technique for cleaning contaminated soil (see [9] and the references therein). The process typically involves an organic pollutant (labeled as a substrate), a nutrient (labeled as an electron acceptor), and indigenous microorganisms. Roughly speaking, when both the substrate and acceptor are present, the microorganisms consume the acceptor and degrade the substrate, decontaminating the soil. Bioremediation involves complex interactions and has many controlling factors that make it difficult to understand. Mathematical analysis of simplified models may allow for the identification of key components which control the behavior of the system, allowing for more effective implementation.
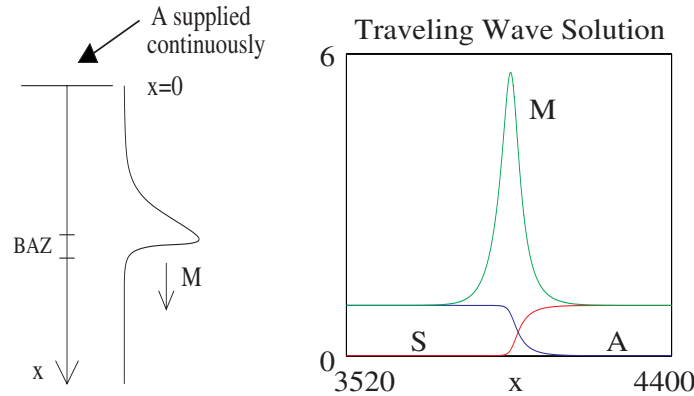
Fig. 1. A schematic diagram of the soil column and the M component of the traveling wave is shown on the left. The traveling wave, observed in numerical simulations in [9] with $a_1 = 0.011$, $a_2 = 0.345$, $a_3 = 0.0885$, $a_4 = 0.0218$, $R_d = 3$, and $K_S = K_A = 0.3$, is shown on the right. S increases from 0 to 1, while A decreases from 1 to 0.

In this article, we study the nondimensional form of the Oya-Valocchi bioremediation model in [9], [6], and [13]. This is a conceptual model that was developed in order to better identify key controlling factors, and also to help connect laboratory work with field experiments [9]. The situation is idealized to be a one-dimensional, semi-infinite soil column with initial constant background level of substrate and of biomass of the microorganisms, but no acceptor. Beginning at time $t = 0$, a constant level of acceptor is injected continuously at the surface of the soil column. This creates a concentration profile of the acceptor that is a traveling front propagating down the soil column, connecting the positive (injection) concentration behind the front and the zero concentration ahead of it. By contrast, the traveling profile of the substrate concentration connects the zero (completely remediated) level behind the front to the constant (initial, undisturbed) level ahead of it. Moreover, the substrate front lags slightly behind that of the acceptor, so that there is a region of overlap between the fronts. In this region, known as the biologically active zone (BAZ), the microbial population is highly elevated due to the supply of both nutrient and substrate. As the fronts move downstream, the location of the elevated microbial population moves with them, and after the fronts pass a given location, the biomass population returns to its equilibrium level. Thus, the biomass concentration exhibits a single bump profile that travels with the fronts as the reaction progresses down the column. See Figure 1.

Two structural assumptions are incorporated into the model. First, the microbes are attached to particles in the soil and therefore do not move. Second, the acceptor is nonsorbing, meaning it travels through the column at the pore water velocity (which has been normalized to be 1), whereas the substrate is sorbing, traveling at the retarded velocity $\frac{1}{R_d}$ where the retardation factor satisfies $R_d > 1$.

Mathematically, we let $S = S(x, t)$, $A = A(x, t)$, and $M = M(x, t)$ denote the concentrations of the substrate, acceptor, and microorganisms, respectively. The model

equations we study are

$$R_d \frac{\partial S}{\partial t} - \frac{\partial^2 S}{\partial x^2} + \frac{\partial S}{\partial x} = -a_1 f_{bd},$$

$$\frac{\partial A}{\partial t} - \frac{\partial^2 A}{\partial x^2} + \frac{\partial A}{\partial x} = -a_1 a_2 f_{bd},$$

$$\frac{\partial M}{\partial t} = a_3 f_{bd} - a_4(M - 1), \tag{1}$$

$$f_{bd} = M \left(\frac{S}{K_S + S} \right) \left(\frac{A}{K_A + A} \right),$$

for $x \in \mathbb{R}$, $t > 0$, in which the diffusion coefficients have been scaled to 1 (see remark 2.3). Because we are interested in traveling waves, the asymptotic conditions are

$$S(-\infty, t) = 0, \qquad A(-\infty, t) = 1, \qquad M(-\infty, t) = 1,$$

$$S(+\infty, t) = 1, \qquad A(+\infty, t) = 0, \qquad M(+\infty, t) = 1. \tag{2}$$

The reaction function f_{bd} represents Monod reaction kinetics. The magnitude of this reaction function is directly proportional to the product of the substrate and acceptor concentrations. Moreover, there is a saturation effect controlled by the parameters K_S and K_A. These are referred to as the relative half-saturation constants for the substrate and acceptor and indicate the degree to which the presence of each (or lack thereof) may limit the growth of the microorganisms. For example, if $K_S \ll 1$, then $\frac{S}{K_S + S} \approx 1$, and the substrate has little effect on microbial growth in the reaction zone, except near the trailing edge of the substrate front where $S < K_S$. However, if $K_S \gg 1$, then $\frac{S}{K_S + S}$ is small, and everywhere the substrate limits microbial growth. Thus, the magnitudes of these quantities will be important in determining the dynamics of the reaction.

The parameters a_i represent ratios of various timescales of the reaction. As explained in [9], a_1 represents the ratio between the transport timescale and the biodegradation timescale of substrate. Similarly, the combined parameter $a_1 a_2$ represents the corresponding ratio for the acceptor. The parameters a_3 and a_4 are the ratios of the transport timescale to the maximum cell growth and cell decay of the microorganisms, respectively.

Finally, the asymptotic conditions (2) may be explained as follows. The asymptotic conditions at $-\infty$ represent the fact that, behind the BAZ, the substrate has been completely degraded, the acceptor level is equal to its injection level, and the microorganism population has returned to its equilibrium level. At $+\infty$, ahead of the BAZ, the soil remains undisturbed and contaminated, and thus the substrate, acceptor, and microorganisms are all equal to their initial levels.

It is of interest to note that the boundary and initial conditions corresponding to the soil column experiment (for $x \in [0, \infty)$ and $t > 0$) are

$$\left(-\frac{\partial S}{\partial x} + S \right)_{x=0} = 0, \qquad \left(-\frac{\partial A}{\partial x} + A \right)_{x=0} = 1,$$

$$S(x, 0) = 1, \quad A(x, 0) = 0, \quad M(x, 0) = 1, \tag{3}$$

and that one should use these to study the initial formulation of the traveling wave. In this case, the boundary conditions for S and A at $x = 0$ represent the fact that a constant

level of acceptor is injected continuously there, while no substrate is added to the system. Here, as written above, we assume the traveling wave has already formed.

Traveling waves of the type shown in Figure 1 have been investigated in [5], [6], [9], and [13]. A dimensional version of (1) was developed in [7], [8], and [12], and further studied in [9], wherein the nondimensional version (1) was derived. These authors carried out an extensive numerical investigation of the model, discovering the traveling wave. In addition, they investigated the effects of varying the parameters K_S and K_A, noting that for some values the traveling wave is stable, while for others there is a stable, time-periodic traveling wave. In this work, the authors were the first to exploit mathematically traveling waves in a bioremediation model in order to determine the substrate removal rate.

Further analysis of the dimensional model was carried out in [6]. In this work, the authors proved the existence of the traveling wave for $R_d > 1$, and positive values of the other parameters. Working with an elliptically regularized form of the dimensional model on a finite domain and using topological degree theory, the authors construct the traveling wave as the fixed point of an appropriate map. Existence is then proven by extending the result to the original, nonelliptic model on the infinite line. In the process, bounds on all three components of the solution are obtained, in particular, an explicit bound on the peak height of the M pulse in terms of the dimensional parameters.

In [13], the transition between the traveling wave behavior and the time-periodic traveling wave behavior, first discovered in [9], is investigated. The authors study the dimensional model in the absence of diffusion using a relaxation procedure and WKB analysis. Using a reduced, two-component model, the authors explicitly determine the traveling wave and show it is stable for certain parameter values, losing stability in an oscillatory fashion.

Ultimately we would like to gain a better mathematical understanding of the mechanism that causes this loss of stability. A geometric construction of the traveling wave will help in this understanding. The geometric structures underlying a traveling wave solution, and how these structures vary with the parameters, provide direct insight into mechanisms governing its stability.

In this paper, we provide a geometric construction of the traveling wave solution for sufficiently large (relative to a singular perturbation parameter δ) values of the half-saturation constants, K_S and K_A. In this parameter regime it will be shown that the entire traveling wave lies on a three-dimensional slow manifold within the five-dimensional phase space of the traveling wave ODE system. Within this slow manifold, the wave will be constructed in the transverse intersection of appropriate stable and unstable manifolds.

In addition to providing further insight into the bioremediation model, this construction is mathematically interesting because of the nonlinear reaction term f_{bd}. Two components of the function, $(\frac{S}{S+K_S})$ and $(\frac{A}{A+K_A})$, have derivatives that become large as K_S and K_A become small. In other words, because the half-saturation constants are scaled so that $K_{S,A} \to 0$ as $\delta \to 0$, the reaction term is not uniformly bounded in the C^1 topology as $\delta \to 0$. This prevents a direct application of Fenichel theory [2], thus preventing one from concluding that geometric structures that are present in the phase space of the model in the asymptotic limit persist. In order to overcome this difficulty, we change coordinates by compactifying the S and A directions in a manner that naturally reflects the components of the reaction function.

As mentioned above, this construction is only valid for large values of the half-saturation constants (relative to δ). For small values of the half-saturation constants, it will be shown that a different analysis is necessary. As we will see, this is because the geometry of the phase space changes significantly as the half-saturation constants decrease through a critical scaling with respect to δ. The parameter regime including smaller values of the half-saturation constants is where the bifurcation to a periodic traveling wave has been observed numerically. Using the moving grid scheme in [1], we will explore numerically this parameter regime, including the bifurcation, and discuss how the geometry of the phase space changes in this case.

The paper is organized as follows. In Section 2, we reformulate the model in terms of a moving coordinate frame that is appropriate to the study of traveling waves. In addition, we derive scalings of the parameters based on the numerical values used in [9] in terms of a small quantity δ, placing the problem within the context of geometric singular perturbation theory. In Section 3, we present the geometric construction of the traveling wave solution for sufficiently large values of the half-saturation constants. In Section 4, we show that the asymptotics for the traveling wave solution agree with the results obtained from numerical simulations, where we note that the asymptotics have been carried out to include both the leading-order terms and the first-order corrections. Finally, in Section 5, we investigate numerically the bifurcation the traveling wave undergoes for small values of the half-saturation constants.

2. Scalings for Traveling Waves

We are interested in traveling wave solutions representing an advancing front for the acceptor A, a trailing front for the substrate S, and a pulse for the biomass M. Plugging the Ansatz

$$s = S(x - ct), \qquad a = A(x - ct), \qquad m = M(x - ct)$$

into (1), we find that the system becomes

$$
\begin{aligned}
s'' + (cR_d - 1)s' &= a_1 f_{bd}, \\
a'' + (c - 1)a' &= a_1 a_2 f_{bd}, \\
cm' &= a_4(m - 1) - a_3 f_{bd},
\end{aligned}
\tag{4}
$$

where $'$ denotes differentiation with respect to the moving coordinate $\xi \equiv x - ct$. The asymptotic conditions are

$$
\begin{aligned}
s(-\infty) &= 0, & s(+\infty) &= 1, \\
a(-\infty) &= 1, & a(+\infty) &= 0, \\
m(-\infty) &= 1, & m(+\infty) &= 1.
\end{aligned}
\tag{5}
$$

Note that these conditions also imply that $s'(\pm\infty) = a'(\pm\infty) = m'(\pm\infty) = 0$.

From the s and a equations in (4), one may compute analytically the wave speed c. To do this, eliminate the term f_{bd} from the equations and integrate once with respect

to ξ. Using the asymptotic conditions, we find

$$c = \frac{a_2 + 1}{a_2 R_d + 1}. \tag{6}$$

As mentioned in [9] and [6], the wave speed depends only on the relative rates of consumption of the substrate and acceptor by the microorganisms (a_2), and the amount of sorbtion of the substrate (R_d). The wave speed is independent of both the microbial parameters (a_3 and a_4), and also of a_1.

Traveling waves are observed numerically in [9] for the following parameter values:

$$a_1 = 0.011, \qquad a_2 = 0.3450, \qquad a_3 = 0.0885, \qquad a_4 = 0.0218, \qquad R_d = 3.0,$$

and a range of values of K_S and K_A. The differences in magnitudes of these parameters suggest that we introduce a small parameter δ and scale the parameters in terms of this quantity. In turn, this will allow us to use singular perturbation theory to determine the mechanisms that produce the observed traveling wave behavior. Moreover, the above values suggest rescaling the parameters as

$$a_1 = \delta^2 \tilde{a}_1, \qquad a_2 = a_2, \qquad a_3 = \delta \tilde{a}_3, \qquad a_4 = \delta^2 \tilde{a}_4, \qquad R_d = R_d. \tag{7}$$

Here $\tilde{a}_1$, $\tilde{a}_3$, and $\tilde{a}_4$ are assumed to be $\mathcal{O}(1)$ with respect to δ.

From numerical simulations, we see that the properties of the traveling wave depend significantly on the half-saturation constants K_S and K_A, and we are interested in a range of values. Specifically, we scale them as

$$K_S = \delta^\kappa \tilde{K}_S, \qquad K_A = \delta^\kappa \tilde{K}_A. \tag{8}$$

Inserting the rescaled quantities into (4) and writing the equations as a system of five first-order equations, we obtain

$$
\begin{aligned}
s' &= v, \\
v' &= -(cR_d - 1)v + \delta^2 \tilde{a}_1 f_{bd}, \\
a' &= r, \\
r' &= -(c - 1)r + \delta^2 \tilde{a}_1 a_2 f_{bd}, \\
m' &= \delta^2 \frac{\tilde{a}_4}{c}(m - 1) - \delta \frac{\tilde{a}_3}{c} f_{bd}.
\end{aligned} \tag{9}
$$

These are the equations we will analyze throughout the rest of the paper.

We will construct the traveling wave for $0 < \kappa < 1$ in Section 3, examine its properties in Section 4, and report on numerical simulations in the regime $\kappa \geq 1$, in which a Hopf bifurcation takes place, in Section 5. The approach in Section 3 can be extended naturally to include the threshold cases $\kappa = 0$ and $\kappa = 1$, although certain technical details are different. In the simulations of [9], the case $\kappa < 0$, i.e. $K_S, K_A \gg 1$, has been considered briefly. The waves observed in this case can also be constructed using an analytical approximation procedure, which is in fact more straightforward since the reaction term is regular (in the C^1 topology) as $\delta \to 0$. We do not consider this case in any further detail here.

Remark 2.1. We have also explored other scalings, such as setting $a_2 = \sqrt{\delta} \tilde{a}_2$ and $R_d = \frac{1}{\sqrt{\delta}} \tilde{R}_d$, as would be suggested by taking $\delta = 0.1$; however, there are various reasons for assuming both are $\mathcal{O}(1)$. These include keeping the reaction terms in the equations for v and r in (9) of the same order and also keeping the terms $(cR_d - 1)$ and $(c - 1)$ in (9) of the same order. In addition, this allows us to retain as many terms as possible, i.e. to find a significant degeneration of the system.

Remark 2.2. In both [9] and [6], it was shown that the assumption that the retardation factor satisfies $R_d > 1$ is crucial for the existence of traveling waves. Biologically this can be understood as providing a mechanism to increase the width of the BAZ. Because the substrate is sorbing, it lags behind after the initial injection of the acceptor before the substrate front begins moving downstream with that of the acceptor. If the retardation factor was not present (i.e. if the substrate was not sorbing), then this lag would not occur and the BAZ would be too narrow to allow an appreciable amount of substrate to be degraded as the reaction progressed downstream.

From the above analysis, one can begin to see mathematically why it is necessary that at least $R_d \neq 1$. If $R_d = 1$, then we would have $c = 1$, and hence the quantities $(c - 1)$ and $(cR_d - 1)$ in equation (9) would both be 0. Therefore, if the substrate was not sorbing, the advection terms would effectively drop out, which would dramatically change the following analysis and also the observed dynamics.

Remark 2.3. We have implicitly chosen the diffusion coefficients in system (1) to be equal and scaled them to 1. It may be possible to extend our analysis to the case where they are not equal. In addition, in both [9] and [6], the dimensional model with zero diffusion was investigated. It was shown that, in this case, a traveling wave solution still exists. It is interesting to note that setting the dimensional diffusion coefficient to zero is equivalent to setting the parameters a_1, a_3, and a_4 equal to zero, while also rescaling space (x) and time (t). See the transformation between the dimensional and nondimensional coordinates in [9] for more details.

3. Geometric Construction of the Traveling Wave

The goal of this section is to prove the following theorem:

Theorem 3.1. *There exists a $\delta_0 > 0$ such that for all $\delta \in (0, \delta_0)$, for all $\kappa \in (0, 1)$, and for all $\tilde{a}_1, a_2, \tilde{a}_3, \tilde{a}_4, \tilde{K}_S, \tilde{K}_A$, and R_d $\mathcal{O}(1)$ and positive, system (9) has a traveling wave solution, $\gamma_{tw}(\xi) = (s_{tw}, v_{tw}, a_{tw}, r_{tw}, m_{tw})(\xi)$, connecting $(s, v, a, r, m) = (0, 0, 1, 0, 1)$ at $-\infty$ with $(s, v, a, r, m) = (1, 0, 0, 0, 1)$ at $+\infty$. In addition, let*

$$\mathcal{L}^- = \left\{ (s, a, m) = (0, 1, m) \quad | \quad m \in \left[1, 1 + \delta^{-1} \frac{\tilde{a}_3(R_d - 1)}{\tilde{a}_1(a_2 + 1)} \right] \right\},$$

and

$$\mathcal{I} = \left\{ (s, a, m) = \left(s, 1 - s, 1 + \delta^{-1} \frac{\tilde{a}_3(R_d - 1)}{\tilde{a}_1(a_2 + 1)} (1 - s) \quad | \quad s \in [0, 1] \right) \right\}.$$

Then the s, a, and m components of the traveling wave are $\mathcal{O}(\delta)$ close to $\mathcal{S}_\delta \equiv \mathcal{L}^- \bigcup \mathcal{I}$.

The theorem states that, to leading order, the traveling wave is the union of $\mathcal{L}^-$ and $\mathcal{I}$. These two curves can be understood biologically as follows. $\mathcal{L}^-$ corresponds to the portion of the traveling wave to the left of the BAZ, where s and a are equal to their asymptotic values at $-\infty$ and m is slowly decaying to its equilibrium value (as $\xi \to -\infty$). Moreover, the constant $1 + \delta^{-1} \frac{\tilde{a}_3(\tilde{R}_d - 1)}{\tilde{a}_1(a_2 + 1)}$ is, to leading order, the maximum value of the microorganism population.

The curve $\mathcal{I}$ corresponds to the portion of the traveling wave inside the BAZ, in which m decays from its maximum value to its asymptotic value at $+\infty$, and s and a transition from their asymptotic values at $-\infty$ to those at $+\infty$. $\mathcal{I}$ also contains the portion of the wave that lies to the right of the BAZ, namely, the point $(1, 0, 1)$.

As we will see below, these two pieces of the traveling wave correspond to portions of the wave that evolve on different timescales. The dynamics on $\mathcal{I}$ occurs on a slow, $\mathcal{O}(\delta)$, timescale, and the dynamics on $\mathcal{L}^-$ occurs on a super-slow, $\mathcal{O}(\delta^2)$, timescale. This separation of timescales is due to the fact that the timescale of the reaction, which is governed by the magnitude of the reaction function $\delta \tilde{a}_i f_{bd}$, is different from the timescale of the intrinsic dynamics of the microorganisms, given by the parameter $\delta^2 \tilde{a}_4$.

It will be shown below that there exist both a slow and a super-slow invariant manifold in the phase space of (9). The leading-order slow system is integrable, and $\mathcal{I}$ corresponds to one of the integral curves. The leading-order super-slow dynamics consist of invariant lines in the phase space where the only dynamic variable is m. The curve $\mathcal{L}^-$ is one of these invariant lines.

The proof of this theorem employs geometric singular perturbation theory to demonstrate that there is a transverse intersection of invariant manifolds in system (9) in which the traveling wave lies.

3.1. Boundedness of the Vector Field in the C^1 Topology

The kinetic terms $\frac{s}{K_S + s}$ and $\frac{a}{K_A + a}$ in f_{bd}, with $K_{S,A} = \delta^\kappa \tilde{K}_{S,A}$ and $\kappa > 0$, are not uniformly bounded in the C^1 topology as $\delta \to 0$. More precisely,

$$\frac{d}{ds}\left(\frac{s}{\delta^\kappa \tilde{K}_S + s}\right) = \frac{\delta^\kappa \tilde{K}_S}{(s + \delta^\kappa \tilde{K}_S)^2} \to \infty \quad \text{for} \quad s \ll \mathcal{O}(\delta^{\kappa/2}).$$

Hence, the perturbation terms in (9) are not uniformly bounded in the C^1 topology, and some preparation of the equations is required before geometric singular perturbation theory [2] – [4] can be applied.

We introduce the new dependent variables,

$$y = \frac{s}{K_S + s}, \qquad w = \frac{a}{K_A + a}, \tag{10}$$

with inverse coordinate change being given by $s = y K_S/(1 - y)$ and $a = w K_A/(1 - w)$. This coordinate change compactifies the s and a directions in the phase space in a manner that naturally reflects the component functions of the reaction function. In terms of these

new variables, system (9) becomes

$$y' = \frac{v}{K_S}(1-y)^2,$$

$$v' = -(cR_d - 1)v + \delta^2 \tilde{a}_1 myw,$$

$$w' = \frac{r}{K_A}(1-w)^2,$$

$$r' = -(c-1)r + \delta^2 \tilde{a}_1 a_2 myw,$$

$$m' = \delta^2 \frac{\tilde{a}_4}{c}(m-1) - \delta \frac{\tilde{a}_3}{c} myw. \tag{11}$$

Numerically, the variables v and r remain small along the traveling wave, while the height of the peak in m is large. For $0 < \kappa < 1$, these numerics suggest scaling $v = \delta^{1+\kappa}\tilde{v}$, $r = \delta^{1+\kappa}\tilde{r}$, and $m - 1 = \delta^{\kappa-1}\tilde{m}$ (see Remark 3.2). Hence, taking into account the scalings of K_S and K_A in (8), we see that system (11) becomes

$$y' = \delta \frac{\tilde{v}}{\tilde{K}_S}(1-y)^2,$$

$$\tilde{v}' = -(cR_d - 1)\tilde{v} + \tilde{a}_1 \tilde{m} yw + \delta^{1-\kappa}\tilde{a}_1 yw,$$

$$w' = \delta \frac{\tilde{r}}{\tilde{K}_A}(1-w)^2,$$

$$\tilde{r}' = -(c-1)\tilde{r} + \tilde{a}_1 a_2 \tilde{m} yw + \delta^{1-\kappa}\tilde{a}_1 a_2 yw,$$

$$\tilde{m}' = -\delta \frac{\tilde{a}_3}{c}\tilde{m} yw - \delta^{2-\kappa}\frac{\tilde{a}_3}{c} yw + \delta^2 \frac{\tilde{a}_4}{c}\tilde{m}. \tag{12}$$

System (12) is the fast-slow system that we will use throughout the proof of Theorem 3.1. We remark that $\delta \ll \delta^{1-\kappa}$, because we are assuming $0 < \kappa < 1$. This will be crucial in the following analysis.

3.2. Geometry of the Fast-Slow System (12)

In system (12), $\tilde{v}$ and $\tilde{r}$ are fast variables, while the rest are slow. The reduced slow system is obtained from (12) by changing the independent variable to the slow time $\eta = \delta\xi$ and by setting $\delta = 0$,

$$y_\eta = \frac{\tilde{v}}{\tilde{K}_S}(1-y)^2,$$

$$0 = -(cR_d - 1)\tilde{v} + \tilde{a}_1 \tilde{m} yw,$$

$$w_\eta = \frac{\tilde{r}}{\tilde{K}_A}(1-w)^2,$$

$$0 = -(c-1)\tilde{r} + \tilde{a}_1 a_2 \tilde{m} yw,$$

$$\tilde{m}_\eta = -\frac{\tilde{a}_3}{c}\tilde{m} yw. \tag{13}$$

The algebraic constraints in (13) imply that $\tilde{v} = -\tilde{r} = \frac{\tilde{a}_1}{cR_d-1}\tilde{m}yw$, where we note that we have used the fact that $a_2(cR_d - 1) = -(c - 1)$. Therefore, system (13) has an invariant manifold given by

$$\mathcal{M}_0 = \left\{ \tilde{v} = -\tilde{r} = \frac{\tilde{a}_1}{cR_d - 1}\tilde{m}yw \right\}, \tag{14}$$

and in this case, since $\delta = 0$, we label $\mathcal{M}_0$ as a critical manifold.

Setting $\delta = 0$ in system (12), we see that the reduced fast dynamics are given by

$$
\begin{aligned}
y' &= 0, \\
\tilde{v}' &= -(cR_d - 1)\tilde{v} + \tilde{a}_1\tilde{m}yw, \\
w' &= 0, \\
\tilde{r}' &= -(c - 1)\tilde{r} + \tilde{a}_1 a_2 \tilde{m}yw, \\
\tilde{m}' &= 0.
\end{aligned}
\tag{15}
$$

Because $cR_d - 1 > 0$ and $c - 1 < 0$, we see that $\tilde{v}$ is decaying exponentially while $\tilde{r}$ is growing exponentially. Hence, $\mathcal{M}_0$ is normally hyperbolic.

Fenichel theory [2], [3], [4] implies that, for sufficiently small δ, the full system (12) has a locally invariant slow manifold, $\mathcal{M}_\delta$, which is C^1 $\mathcal{O}(\delta^{1-\kappa})$ close to $\mathcal{M}_0$. In addition, $\mathcal{M}_\delta$ is the graph of a function, which has a regular perturbation expansion, as follows:

$$
\begin{aligned}
\tilde{v} &= h_0(\tilde{m}, y, w) + \delta^{1-\kappa}h_1(\tilde{m}, y, w) + \delta h_2(\tilde{m}, y, w) + \text{h.o.t}, \\
\tilde{r} &= g_0(\tilde{m}, y, w) + \delta^{1-\kappa}g_1(\tilde{m}, y, w) + \delta g_2(\tilde{m}, y, w) + \text{h.o.t}.
\end{aligned}
\tag{16}
$$

The functions h_i and g_i, $i = 0, 1, 2$, are obtained by computing $d\tilde{v}/d\xi$ and $d\tilde{r}/d\xi$ from the above asymptotic expansion and from system (12), respectively, and then by equating these two expressions, which expresses analytically the invariance of $\mathcal{M}_\delta$. By using (6), at $\mathcal{O}(1)$, we find

$$
\begin{aligned}
h_0 &= \frac{\tilde{a}_1}{(cR_d - 1)}\tilde{m}yw, \\
g_0 &= -h_0.
\end{aligned}
\tag{17}
$$

At $\mathcal{O}(\delta^{1-\kappa})$, we find

$$
\begin{aligned}
h_1 &= \frac{\tilde{a}_1}{(cR_d - 1)}yw, \\
g_1 &= -h_1.
\end{aligned}
\tag{18}
$$

Finally, at $\mathcal{O}(\delta)$,

$$
\begin{aligned}
h_2 &= -\frac{\tilde{a}_1^2}{(cR_d - 1)^3}yw\tilde{m}\left\{ \frac{\tilde{m}w(1 - y)^2}{\tilde{K}_S} - \frac{\tilde{m}y(1 - w)^2}{\tilde{K}_A} - \frac{\tilde{a}_3(cR_d - 1)}{c\tilde{a}_1}yw \right\}, \\
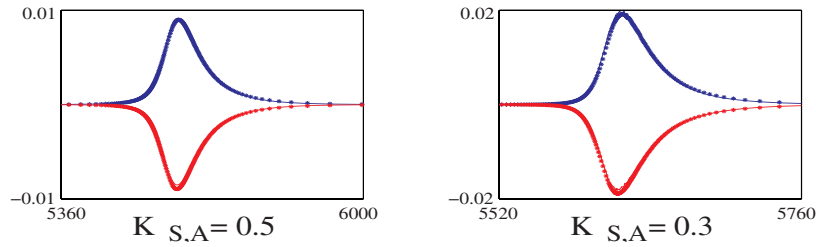g_2 &= \frac{1}{a_2}h_2.
\end{aligned}
\tag{19}
$$

Fig. 2. A comparison of $\tilde{v}$ (upper curve) and $\tilde{r}$ (lower curve) as computed numerically (*) and using the asymptotic expansion (-) given by equation (16), for $K_{S,A} = 0.5$ and $K_{S,A} = 0.3$.

The equations for $\tilde{v}$ and $\tilde{r}$ in (15) indicate that if a solution were to leave the slow manifold it would not return and either $\tilde{v}$ or $\tilde{r}$ would tend to infinity as $\xi \to \pm\infty$. Therefore, the entire traveling wave solution must be contained within the slow manifold.

Numerical verification of the asymptotic expansions given in equation (16) is shown in Figure 2. Note the good agreement as expected for $0 < \kappa < 1$.

Remark 3.2. The reason for choosing the scalings $v = \delta^{1+\kappa}\tilde{v}$, $r = \delta^{1+\kappa}\tilde{r}$, and $m - 1 = \delta^{\kappa-1}\tilde{m}$ can be seen as follows. First, the numerics indicate that the reaction term balances with v and r along the wave for $0 < \kappa < 1$, and under these scalings, it is precisely these terms that are $\mathcal{O}(1)$ in the right members of the equations for $\tilde{v}$ and $\tilde{r}$ in (11) when the above scalings are employed. Second, y', w', and $\tilde{m}'$ are of the same order in (12), as are $\tilde{v}'$ and $\tilde{r}'$. This allows for the reduction to the three-dimensional slow manifold $\mathcal{M}_\delta$.

3.3. Dynamics on the Slow Manifold $\mathcal{M}_\delta$

The dynamics on the slow manifold $\mathcal{M}_\delta$ are obtained by inserting formulas (16) into system (12) and changing the independent variable to the slow time $\eta = \delta\xi$,

$$y_\eta = \frac{(1-y)^2}{\tilde{K}_S}[h_0 + \delta^{1-\kappa}h_1 + \delta h_2 + \mathcal{O}(\delta^{2-\kappa})],$$

$$w_\eta = \frac{(1-w)^2}{\tilde{K}_A}[g_0 + \delta^{1-\kappa}g_1 + \delta g_2 + \mathcal{O}(\delta^{2-\kappa})],$$

$$\tilde{m}_\eta = -\frac{\tilde{a}_3}{c}\tilde{m}yw - \delta^{1-\kappa}\frac{\tilde{a}_3}{c}yw + \delta\frac{\tilde{a}_4}{c}\tilde{m}. \tag{20}$$

Retaining the $\mathcal{O}(1)$ and $\mathcal{O}(\delta^{1-\kappa})$ terms, we have

$$y_\eta = \frac{\tilde{a}_1}{\tilde{K}_S(cR_d - 1)}(1-y)^2[\tilde{m}yw + \delta^{1-\kappa}yw],$$

$$w_\eta = -\frac{\tilde{a}_1}{\tilde{K}_A(cR_d - 1)}(1-w)^2[\tilde{m}yw + \delta^{1-\kappa}yw],$$

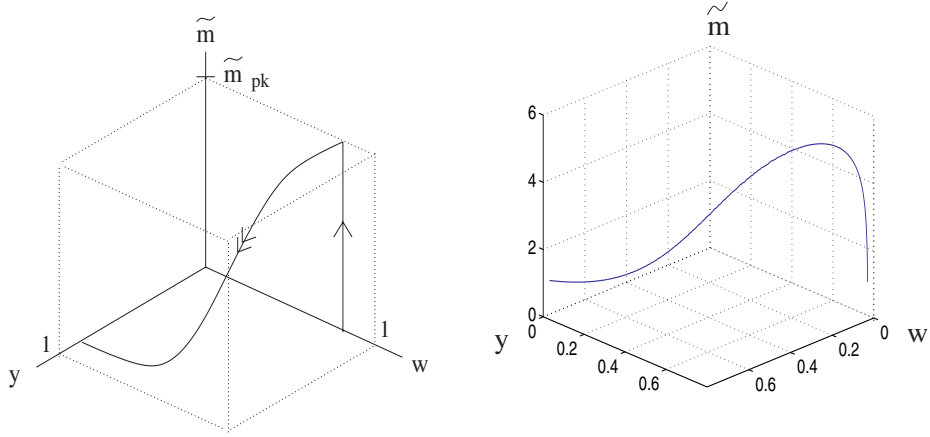$$\tilde{m}_\eta = -\frac{\tilde{a}_3}{c}[\tilde{m}yw + \delta^{1-\kappa}yw]. \tag{21}$$

Fig. 3. On the left is a sketch of an integral curve for system (21) near the TW solution. Here $\tilde{m}_{pk}$ is the height of the peak in $\tilde{m}$, as given in equation (32). A plot of the numerically computed traveling wave is shown on the right, for $K_{S,A} = 0.3$.

In turn, from (21) we see that up to terms of $\mathcal{O}(\delta)$,

$$\frac{\tilde{K}_S}{(1-y)^2} y_\eta = -\frac{\tilde{K}_A}{(1-w)^2} w_\eta = -\frac{c\tilde{a}_1}{\tilde{a}_3(cR_d - 1)} \tilde{m}_\eta. \tag{22}$$

Integrating these equalities pairwise, we find that the integral curves of (21) are given by

$$c_0 = \frac{\tilde{K}_S}{1-y} + \frac{\tilde{K}_A}{1-w},$$

$$\tilde{m} = \frac{\tilde{a}_3(cR_d - 1)}{c\tilde{a}_1} \left(\frac{\tilde{K}_A}{1-w} + c_1 \right),$$

$$\tilde{m} = \frac{\tilde{a}_3(cR_d - 1)}{c\tilde{a}_1} \left(-\frac{\tilde{K}_S}{1-y} + c_2 \right), \tag{23}$$

where c_i, $i = 0, 1, 2$ are arbitrary constants that determine which integral curve the solution is on. Moreover, we see that $c_0 + c_1 = c_2$, by equating the two expressions for $\tilde{m}$. Hence, (22) determines a two-parameter family of independent integral curves.

   To identify the integral curve corresponding to the traveling wave whose existence we want to establish, we use the full ($\delta > 0$) boundary conditions $y(+\infty) = \frac{1}{1+\delta^\kappa \tilde{K}_S}$ and $w(+\infty) = 0$, as well as $y(-\infty) = 0$ and $w(-\infty) = \frac{1}{1+\delta^\kappa \tilde{K}_A}$. The integral curve that satisfies these boundary conditions is defined by $\delta^\kappa c_0 = 1 + \delta^\kappa \tilde{K}_S + \delta^\kappa \tilde{K}_A$. In other words, in terms of the y and w variables, the integral curve $\mathcal{I}$, which constitutes part of the traveling wave, is given up to $\mathcal{O}(\delta)$ by

$$\frac{\delta^\kappa \tilde{K}_S}{1-y} + \frac{\delta^\kappa \tilde{K}_A}{1-w} = 1 + \delta^\kappa \tilde{K}_S + \delta^\kappa \tilde{K}_A. \tag{24}$$

Similarly, in y and $\tilde{m}$, this integral curve $\mathcal{I}$ contains the point $(\frac{1}{1+\delta^\kappa \tilde{K}_S}, 0)$ and is given by $\delta^\kappa c_2 = 1 + \delta^\kappa \tilde{K}_S$. Also, we have $\delta^\kappa c_1 = -\delta^\kappa \tilde{K}_A$, since $c_0 + c_1 = c_2$. Therefore, along the integral curve $\mathcal{I}$, $\tilde{m}$ is given as a function of w, respectively y, by

$$\delta^\kappa \tilde{m} = \frac{\tilde{a}_3(cR_d - 1)}{c\tilde{a}_1}\left(\frac{\delta^\kappa \tilde{K}_A}{1-w} - \delta^\kappa \tilde{K}_A\right),$$

$$\delta^\kappa \tilde{m} = \frac{\tilde{a}_3(cR_d - 1)}{c\tilde{a}_1}\left(-\frac{\delta^\kappa \tilde{K}_S}{1-y} + 1 + \delta^\kappa \tilde{K}_S\right). \tag{25}$$

To complete the construction of the traveling wave up to $\mathcal{O}(\delta)$, we append to the integral curve $\mathcal{I}$ the line segment $\mathcal{L}^- = \{(y, w, \tilde{m})| y = 0, w = \frac{1}{1+\delta^\kappa \tilde{K}_A}, \tilde{m} \in [0, \tilde{m}_{pk}]\}$, where $\tilde{m}_{pk}$ is a constant that will be determined explicitly in Section 4. The union

$$\mathcal{S}_\delta = \mathcal{I} \bigcup \mathcal{L}^- \tag{26}$$

is the traveling wave to leading order.

Remark 3.3. The reason for including the $\mathcal{O}(\delta^{1-\kappa})$ terms when determining the leading order traveling wave is that the integral curves (23) become degenerate as $\delta \to 0$.

3.4. Completion of the Proof of Theorem 3.1

In this section, we complete the proof of Theorem 3.1 by identifying certain submanifolds of the slow manifold $\mathcal{M}_\delta$ and by showing that these submanifolds intersect transversely along a one-dimensional curve that is given by the set $\mathcal{S}_\delta$, recall (26), up to $\mathcal{O}(\delta)$. The traveling wave will be the heteroclinic orbit that lies in this transverse intersection.

First, notice that for the full system (12), the manifold $\mathcal{N}_\delta \equiv \mathcal{N}_\delta^- \bigcup \mathcal{N}_\delta^+ = \{y = \tilde{v} = \tilde{r} = 0\} \bigcup \{w = \tilde{r} = \tilde{v} = 0\}$ is invariant for all $\delta \geq 0$. On this manifold, the dynamics of $\tilde{m}$ are given by $\tilde{m}_\xi = \delta^2 \frac{\tilde{a}_4}{c}\tilde{m}$, while y, $\tilde{v}$, w, and $\tilde{r}$ are constant. These dynamics correspond to the behavior of the microorganisms in the absence of any reaction and occur on the "super-slow" timescale which is $\mathcal{O}(\delta^2)$. This suggests that we carry out a fast-slow decomposition of the dynamics within $\mathcal{M}_\delta$.

In fact, $\mathcal{N}_\delta$ is a super-slow manifold for (20). To see this, rewrite the system in terms of the variable $\zeta = \delta\eta$ so that the derivatives balance with the $\mathcal{O}(\delta)$ terms on the right-hand sides. In order to observe these super-slow dynamics, we must have $h_0 + \delta^{1-\kappa}h_1 = 0$. This is true if either $y = 0$ or $w = 0$. Note that these two conditions both imply that $h_2 = g_2 = 0$. Therefore, on $\mathcal{N}_\delta$ the dynamics are given, to leading order, by

$$y_\zeta = 0,$$

$$w_\zeta = 0,$$

$$\tilde{m}_\zeta = \frac{\tilde{a}_4}{c}\tilde{m}. \tag{27}$$

We see that on $\mathcal{N}_\delta^-$, the lines for fixed w are invariant, and $\tilde{m}$ grows exponentially away from 0. Similarly, on $\mathcal{N}_\delta^+$ the lines for fixed y are invariant and $\tilde{m}$ grows exponentially away from 0.
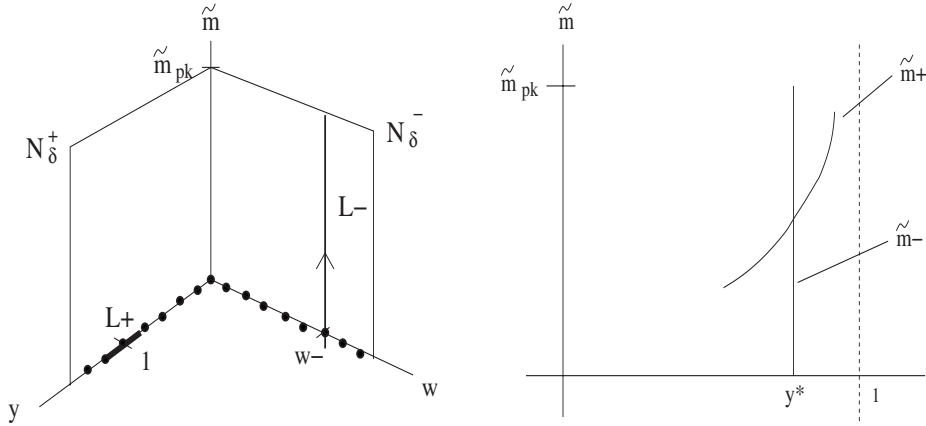
Fig. 4. On the left is a schematic diagram of the phase space of (27), showing the slow manifold $\mathcal{N}_0$ and the lines $\mathcal{L}^{\pm}$. A sketch of the functions $\tilde{m}^-(y)$ and $\tilde{m}^+(y)$ in the plane $\{y = w\}$ showing the transverse intersection is shown on the right, where $y* = \tilde{K}_A w_- / (\tilde{K}_A + \tilde{K}_S - \tilde{K}_S w_-)$.

Consider the line segments

$$\mathcal{L}^- = \{(0, w_-, \tilde{m}): w_-\text{fixed}, \quad \tilde{m} \in [0, \tilde{m}_{pk}]\},$$

$$\mathcal{L}^+ = \left\{(y_+, 0, 0): y_+ \in \left(\frac{1}{1 + \delta^\kappa \tilde{K}_S} - \epsilon, \frac{1}{1 + \delta^\kappa \tilde{K}_S} + \epsilon\right)\right\}, \tag{28}$$

for some $\epsilon > 0$ and a constant $\tilde{m}_{pk}$ which will be defined in Section 4 (see Figure 4). Using the integral curves given in (23), we will track $\mathcal{L}^-$ forward and $\mathcal{L}^+$ backward to the plane $\{y = w\}$ and show that they intersect transversely in this plane.

First, we will track $\mathcal{L}^-$ forward. Any integral curve that intersects $\mathcal{L}^-$ must contain a point of the form $(0, w_-, \tilde{m})$. Using this information we can determine the constants c_0 and c_1 for the integral curves that determine the evolution of $\mathcal{L}^-$. We find that $c_0 = \tilde{K}_S + \frac{\tilde{K}_A}{1-w_-}$ and $c_1 = \frac{c\tilde{a}_1}{\tilde{a}_3(cR_d-1)}\tilde{m} - \frac{\tilde{K}_A}{(1-w_-)}$. This implies that in the plane $\{y = w\}$, by (23), we have

$$y = w = \frac{\tilde{K}_A w_-}{\tilde{K}_A + \tilde{K}_S - \tilde{K}_S w_-}; \quad \tilde{m}^- \in [0, \tilde{m}_{pk}]. \tag{29}$$

We can use a similar procedure to track $\mathcal{L}^+$ backward. Any integral curve intersecting $\mathcal{L}^+$ must contain a point of the form $(y_+, 0, 0)$, which implies that $c_0 = \tilde{K}_A + \frac{\tilde{K}_S}{1-y_+}$ and $c_2 = \frac{\tilde{K}_S}{(1-y_+)}$. Hence, on the plane $\{y = w\}$ we have

$$\tilde{m}^+(y) = \frac{\tilde{K}_A \tilde{a}_3(cR_d-1)}{\tilde{a}_1 c}\left(\frac{y}{1-y}\right); \qquad y \in \left(\frac{1}{1+\delta^\kappa \tilde{K}_S} - \epsilon, \frac{1}{1+\delta^\kappa \tilde{K}_S} + \epsilon\right). \tag{30}$$

Graphs of $\tilde{m}^-(y)$ and $\tilde{m}^+(y)$, which intersect transversely, are shown in Figure 4. Because the images of $\mathcal{L}^-$ and $\mathcal{L}^+$ intersect transversely, we know that a trajectory connecting

the point $(0, w_-, 0)$ and the line $\mathcal{L}^+$ will persist under the addition of the higher order terms [11].

All that remains to be shown is that if we choose $w_- = \frac{1}{1+\delta^\kappa \tilde{K}_A}$, then $y_+ = \frac{1}{1+\delta^\kappa \tilde{K}_S}$. This will result from the following argument. Notice that, using (11),

$$a_2[v' + (cR_d - 1)v] = r' + (c - 1)r.$$

If we use the fact that $y(+\infty) = y_+$, $w(-\infty) = w_-$, and $y(-\infty) = w(+\infty) = 0$, and integrate from $-\infty$ to $+\infty$, we see that

$$a_2(cR_d - 1)\frac{\delta^\kappa \tilde{K}_S y_+}{1 - y_+} = -(c - 1)\frac{\delta^\kappa \tilde{K}_A w_-}{1 - w_-}, \tag{31}$$

and using the fact that $a_2(cR_d - 1) = -(c - 1)$ we see that $y_+ = \frac{\tilde{K}_A w_-}{\tilde{K}_S + (\tilde{K}_A - \tilde{K}_S)w_-}$. Therefore, if we choose $w_- = \frac{1}{1+\delta^\kappa \tilde{K}_A}$, then we must also have $y_+ = \frac{1}{1+\delta^\kappa \tilde{K}_S}$. The reason for this is that the boundary conditions are encoded in the wave speed.

The proof of Theorem 3.1 is completed by rewriting the expression for $\mathcal{I}$ given in equations (24) and (25) in terms of the variables s, a, and m.

Remark 3.4. We briefly comment on the choice of the lines $\mathcal{L}^\pm$. Because $\mathcal{L}^-$ is the unstable manifold of the point $(0, w^-, 0)$ within $\mathcal{N}_0^-$, it is natural to track its forward evolution. Since we are interested in a solution that is asymptotic to a point of the form $(y^+, 0, 0)$, one might initially attempt to track its stable manifold backwards. However, this would then require the transverse intersection of a two-dimensional manifold with a one-dimensional manifold in a three-dimensional phase space, which is, in general, not generic. Thus, we track the stable manifold of the line $\mathcal{L}^+$ backwards, so that both tracked manifolds have dimension two and their intersection is one-dimensional.

4. The Dependence of the Peak Height on K_S and K_A

In this section, we compute the peak height of the $\tilde{m}$ component of the traveling wave first to leading-order and then also up to and including the first-order corrections. First, we determine the leading-order value using equation (25). The maximum value of $\tilde{m}$ will be attained when $y = 0$, or equivalently when $w = \frac{1}{1+\delta^\kappa \tilde{K}_A}$. Thus, we see that the peak height is defined by

$$\delta^\kappa \tilde{m}_{pk} \equiv \frac{\tilde{a}_3(cR_d - 1)}{c\tilde{a}_1} = \frac{\tilde{a}_3(R_d - 1)}{\tilde{a}_1(a_2 + 1)}, \tag{32}$$

where we have used the value of c given in (6).

The value of $\delta^\kappa \tilde{m}_{pk}$ to leading order, $\frac{\tilde{a}_3(R_d-1)}{\tilde{a}_1(a_2+1)}$, is exactly the upper bound on the peak height obtained in [6]. In other words, we have found that their bound is sharp, up to higher-order effects in δ. Note that the bound in [6] is given in terms of the dimensional parameters (see [9] for the relationship between the dimensional and nondimensional parameters).
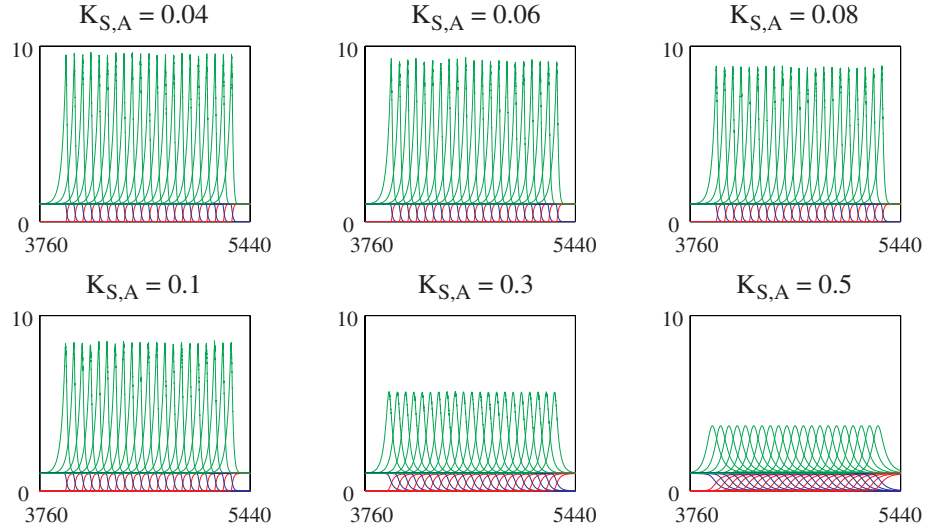
Fig. 5. Plot of the traveling wave, show at successive time steps, for increasing values of the half-saturation constants K_S and K_A. Note that as the half-saturation increase, the height of the peak decreases.

Remark 4.1. In the limit as $\delta \to 0$, $\tilde{m}_{pk} \to \infty$. This is due to the degenerate nature of the integral curves in the singular limit. If we were to define a new variable $\hat{m} = \delta^\kappa \tilde{m}$, then $\hat{m}_{pk}$ would remain $\mathcal{O}(1)$ as $\delta \to 0$, and this would suggest working with the variable $\hat{m}$ throughout the analysis. However, this prevents one from balancing the derivatives of y and w with that of $\hat{m}$ on the slow manifold $\mathcal{M}_\delta$. Therefore, we work with the variable $\tilde{m}$ instead.

Numerically, one observes that the height of the peak in the $\tilde{m}$ component increases as the half-saturation constants K_S and K_A decrease (see Figure 5), as long as one remains in the regime where the traveling wave is stable. This increase is confirmed analytically using the analysis on the slow manifold $\mathcal{M}_\delta$, as we show now.

We compute $d\tilde{m}/dy$ using (20) and the definitions of h_i, and g_i, $i = 0, 1, 2$ given in (17), (18), and (19),

$$\frac{d\tilde{m}}{dy} = -\frac{\tilde{m}_{pk}\tilde{K}_S}{(1-y)^2}\left(\frac{1-\delta f_1(y, w, \tilde{m})}{1-\delta f_2(y, w, \tilde{m})}\right), \tag{33}$$

where f_1 and f_2 are given by

$$f_1(y, w, \tilde{m}) = \frac{\tilde{a}_4}{\tilde{a}_3}\left(\frac{\tilde{m}}{\tilde{m}yw + \delta^{1-\kappa}yw}\right),$$

$$f_2(y, w, \tilde{m}) = \frac{\tilde{a}_1}{(cR_d - 1)^2}\left(\frac{\tilde{m}}{\tilde{m} + \delta^{1-\kappa}}\right)$$

$$\times \left(\frac{\tilde{m}w(1-y)^2}{\tilde{K}_S} - \frac{\tilde{m}y(1-w)^2}{\tilde{K}_A} - \frac{\tilde{a}_3(cR_d - 1)}{c\tilde{a}_1}yw\right). \tag{34}$$
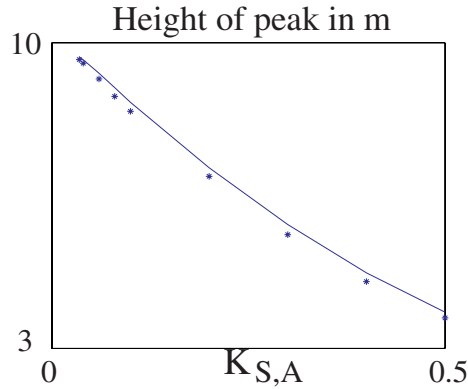
Fig. 6. Graph of the height of the peak in m versus the half-saturation constants K_S and K_A (where $K_S = K_A$) as computed numerically (*) and as computed using the higher-order corrections on the slow manifold $\mathcal{M}_\delta$ (solid curve), via equation (33).

In order that equation given (33) depends only on $\tilde{m}$ and y, we eliminate w using the leading-order integral curve $w = w(y)$ given in (24). That is,

$$w = \frac{(1 + \delta^\kappa \tilde{K}_S)(1 - y) - \delta^\kappa \tilde{K}_S}{(1 + \delta^\kappa \tilde{K}_S + \delta^\kappa \tilde{K}_A)(1 - y) - \delta^\kappa \tilde{K}_S}.$$

Inserting the above expression into the functions f_1 and f_2, we obtain the leading-order differential equation for $\tilde{m}$ in terms of y. Integrating this equation numerically to determine the height of the peak in $\tilde{m}$, we see in Figure 6 that m_{pk} decreases as K_S and K_A increase. In Figure 6, we also see that the analytical results agree with the numerical results, except for some higher-order corrections. This provides further evidence that, for $0 < \kappa < 1$, the entire traveling wave solution really is contained on the three-dimensional slow manifold $\mathcal{M}_\delta$.

5. Bifurcation to Periodic Waves

As previously mentioned, the geometry of system (11) changes when $\kappa > 1$. Most prominently, as κ increases (or K_S and K_A decrease), the traveling wave loses stability to a periodic wave. In this section, we demonstrate this behavior by numerically investigating the bioremediation model.

5.1. Numerical Methods

In order to integrate system (1), we have used a moving grid code which is described in detail in [1]. Because numerical integration must be performed on a finite domain, the simulations have been run for $x \in [0, 10000]$, and the asymptotic conditions given

in (5) have been used as boundary conditions at the endpoints of the spatial interval. This domain is sufficiently large so that the effects of the finite domain are exponentially small in δ over all of the intervals of time of the simulations. The initial data used are as follows. The microorganism concentration, M, was taken to be constant and equal to 1; the substrate concentration, S, was taken to be 1 everywhere except near the left edge, where it linearly decreases to 0; and the acceptor concentration, A, was taken to be 0 everywhere except near the left edge, where it linearly increases to 1.

For all results presented in this section, the parameter values used are

$$a_1 = 0.011, \quad a_2 = 0.3450, \quad a_3 = 0.0885, \quad a_4 = 0.0218, \quad R_d = 3.0, \quad (35)$$

which are the same as those given in Section 2. We remark, however, that the bioremediation model has been numerically integrated for other values of these parameters, to ensure that the traveling wave is not unstable relative to small changes in them.

We are interested in the behavior of system (1) for a range of values of the half-saturation constants. In particular, we have run numerical simulations for $K_S = K_A \in [0.01, 1]$. For this paper we have taken $K_S = K_A$ to simplify the scope of the numerical simulations.

5.2. Geometry of the Phase Space

Based upon the preceding existence construction, we see that for $0 < \kappa < 1$, or $0.1 < K_{S,A} < 1$, the entire traveling wave is contained within a three-dimensional slow manifold within the five-dimensional phase space, given by the asymptotic expansions (16). This was verified numerically in Figure 2.

Similarly, we can see numerically that this is not the case when $\kappa > 1$, or $K_{S,A} < 0.1$, given the values of the other parameters. In other words, if we plot the asymptotic expansion in (16) for $\kappa > 1$ (evaluated using the numerical values of y, w, and $\tilde{m}$) against the values of $\tilde{v}$ and $\tilde{r}$ as computed numerically, we see that they do not agree (see Figure 7). This indicates that the slow manifold $\mathcal{M}_\delta$ no longer contains the traveling wave solution for these parameter values. Because the bifurcation to a periodic wave happens for small values of K_S and K_A, understanding this change in geometry may provide insight into why the traveling wave loses stability.
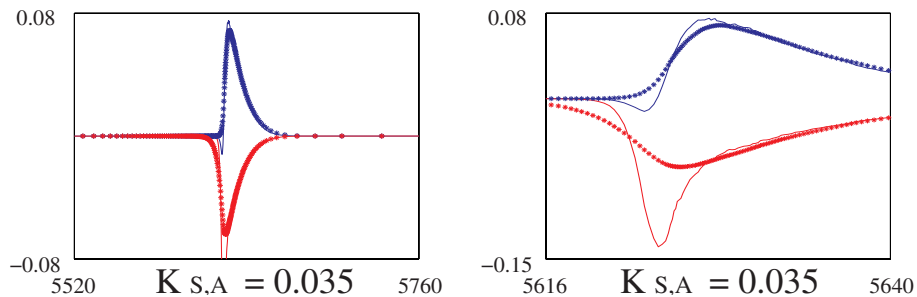

Fig. 7. A comparison of $\tilde{v}$ and $\tilde{r}$ as computed numerically (*) and using the asymptotic expansion (-), for $K_S = K_A = 0.035$. The figure on the right is a close-up of that on the left.
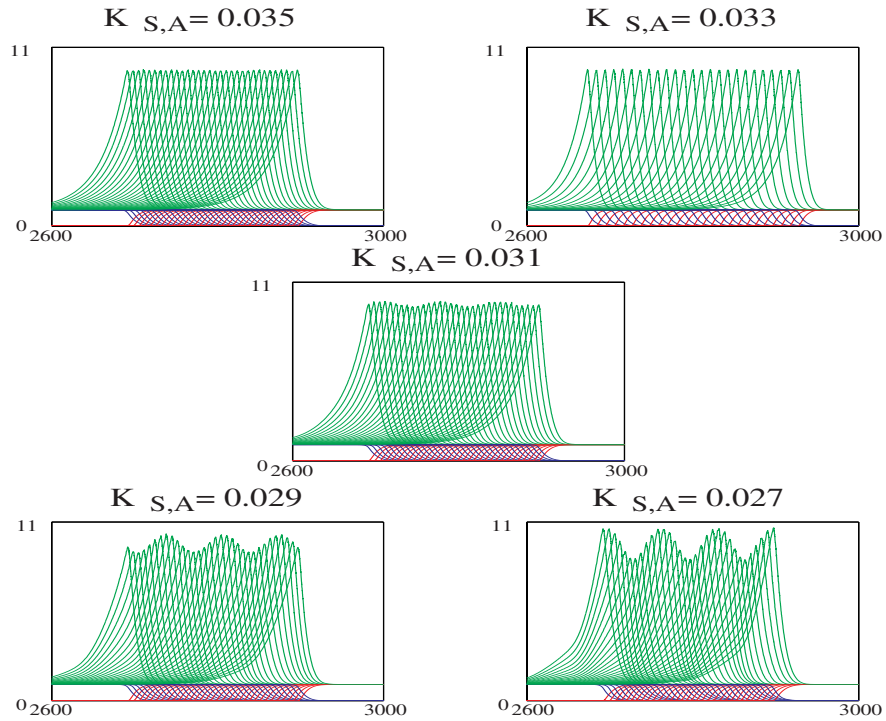
Fig. 8. Each frame shows 33 snapshots of the numerically observed traveling wave at intervals of 10 time units. Note that the traveling wave appears to lose stability to a time-periodic wave approximately for a value of $K_{S,A}$ somewhere inside $(0.031, 0.033)$.

5.3. Periodic Waves

As K_S and K_A decrease further, the traveling wave loses stability to a periodic wave. This bifurcation happens for $K_S = K_A \approx 0.032$, which corresponds to $\kappa \approx 3/2$, and is shown in Figure 8. Each graph shows snapshots of the traveling wave at time intervals of ten units. For values of $K_{S,A}$ below the bifurcation value, the peak height in the m component of the wave varies periodically as the wave travels. Notice that the frequency of oscillation appears to be constant. This suggests that the traveling wave loses stability as the result of a Hopf bifurcation, where two conjugate eigenvalues cross the imaginary axis.

If we approximate the period of oscillation using the numerical results shown in Figure 8, we find that the period is approximately 102.7 nondimensional time units. Consequently, this implies the frequency of oscillation is about $2\pi/102.7 \approx 0.061$. Therefore, we expect that the stability analysis will show that two conjugate eigenvalues cross the imaginary axis with imaginary part near 0.061 as $K_{S,A}$ decrease through 0.032.

In order to verify this numerically observed behavior, stability analysis for the parameter regime in which we have constructed the traveling wave, $0 < \kappa < 1$, must be performed. In addition, construction and stability analysis of the traveling wave in the

regime $\kappa > 1$ needs to be carried out in order to investigate the bifurcation. This is the subject of future work.

6. Conclusions

The traveling wave for the bioremediation model has been constructed for sufficiently large values of the half-saturation constants K_S and K_A. After controlling the nonlinearity with a change of coordinates, we used geometric singular perturbation theory to show that the wave exists on a three-dimensional slow manifold within the five-dimensional phase space. The construction was completed by showing that the leading-order wave exists in the transverse intersection of appropriate stable and unstable manifolds and showing that this transverse intersection persists. We demonstrated that the peak height in the m component of the traveling wave decreases as K_S and K_A increase. In addition, it was shown numerically that the traveling wave loses stability to a periodic wave as the half-saturation constants decrease. Construction of the wave for small values of the half-saturation constants and a complete stability analysis are the subjects of future work.

Acknowledgments

References

[1] J. G. Blom and P. A. Zegeling. Algorithm 731: A moving grid interface for systems of one-dimensional time-dependent partial differential equations. *ACM Transactions on Mathematical Software*, 20(2):194–214, 1994.

[2] N. Fenichel. Persistence and smoothness of invariant manifolds for flows. *Ind. Univ. Math. J.*, 21:193–226, 1971.

[3] N. Fenichel. Geometric singular perturbation theory for ordinary differential equations. *J. Diff. Eq.*, 31(1):53–98, 1979.

[4] C. K. R. T. Jones. Geometric singular perturbation theory. In R. Johnson, editor, *Dynamical Systems*, volume 1609 of *Lecture Notes in Mathematics*, pages 44–118. Springer-Verlag, Berlin, 1994.

[5] H. Keijzer, R. J. Schotting, and S.E.A.T.M. van der Zee. Semi-analytical traveling wave solution of one-dimensional aquifer bioremediation. *Commun. Appl. Numer. Anal.*, 7(1):1–20, 2000.

[6] R. Murray and J. X. Xin. Existence of traveling waves in a biodegradation model for organic contaminants. *SIAM J. Math. Anal.*, 30(1):72–94, 1998.

[7] J. E. Odencrantz. *Modeling the biodegradation kinetics of dissolved organic contaminants in a heterogeneous two-dimensional aquifer*. PhD thesis, University of Illinois, Urbana, 1992.

[8] J. E. Odencrantz, A. J. Valocchi, and B. E. Rittmann. Modeling the interaction of sorption and biodegradation on transport in ground water in situ bioremediation systems. In E. Poeter, S. Ashlock, and J. Proud, editors, *Proceedings of the 1993 Groundwater Modeling Conference*, pages 2-3 to 2-12, Golden, CO, 1993. Int. Ground Water Model. Cent.

[9] S. Oya and A. J. Valocchi. Characterization of traveling waves and analytical estimation of pollutant removal in one-dimensional subsurface bioremediation modeling. *Water Resources Research*, 33(5):1117–1127, 1997.

[10] S. Oya and A. J. Valocchi. Analytical approximation of biodegradation rate for in situ bioremediation of groundwater under ideal radial flow conditions. *J. Contaminant Hydrology*, 31:65–83, 1998.

[11] P. Szmolyan. Transversal heteroclinic and homoclinic orbits in singular perturbation problems. *J. Diff. Eq.*, 92:252–281, 1991.

[12] A. J. Valocchi, J. E. Odencrantz, and B. E. Rittmann. Computational studies of the transport of reactive solutes: Interaction between adsorption and biotransformation. In S. Y. Wang, editor, *Proceedings of the First International Conference on Hydro-Science and Engineering*, vol. 1, pages 1845–1852, Washington, D.C., 1993.

[13] J. X. Xin and J. M. Hyman. Stability, relaxation, and oscillation of biodegradation fronts. *SIAM J. Appl. Math.*, 61(2):472–505, 2000.